AGU ADVANCING EARTH AND SPACE SCIENCES

Earth and Space Science

RESEARCH ARTICLE
10.1029/2023EA003416

Measuring Bedload Motion Time at Second Resolution Using Benford's Law on Acoustic Data

Ci-Jian Yang[1], Jens M. Turowski[2], Qi Zhou[2,3], Ron Nativ[2,4], Hui Tang[2], Jui-Ming Chang[5], and Wen-Sheng Chen[6]

[1]Department of Geography, National Taiwan University, Taipei, Taiwan, [2]Helmholtzzentrum Potsdam, GFZ German Research Center for Geosciences, Potsdam, Germany, [3]Institute of Geosciences, University of Potsdam, Potsdam, Germany, [4]Department of Earth and Environmental Sciences, Ben-Gurion University of the Negev, Be'er Sheva, Israel, [5]Department of Civil Engineering, National Yang Ming Chiao Tung University, Hsinchu, Taiwan, [6]Center for General Education, National Dong Hwa University, Hualien, Taiwan

Abstract Bedload transport is a natural process that strongly affects the Earth's surface system. An important component of quantifying bedload transport flux and establishing early warning systems is the identification of the onset of bedload motion. Bedload transport can be monitored with high temporal resolution using passive acoustic methods, for example, hydrophones. Yet, an efficient method for identifying the onset of bedload transport from long-term continuous acoustic data is still lacking. Benford's Law defines a probability distribution of the first-digit of data sets and has been used to identify anomalies. Here, we apply Benford's law to continuous acoustic recordings from Baiyang hydrometric station, a tributary of Liwu River, Taroko National Park, Taiwan at the frequency of 32 kHz from stationary hydrophones deployed for 3 years since 2019. We construct a workflow to parse sound combinations of bedload transportation and analyze them in the context of hydrometric sensing constraining the onset, and recession of bedload transport. We identified three separate sound classes in the data related to the noise produced by the motion of pebbles, water flow, and air. We identify two bedload transport events that lasted 17 and 45 hr, respectively, covering about 0.35% of the total recorded time. The workflow could be transferred to other different catchments, events, or data sets. Due to the influence of instrument and background noise on the regularity of the residuals of the first-digit, we recommend identifying the first-digit distribution of the background noise and ruling it out before implementing this workflow.

Plain Language Summary Long-term, high-frequency monitoring of Earth surface processes brings huge data sets that can be of high quality. Benford's Law defines the specific probability distribution of the first-digit of the data sets and has been used to identify anomalies and high-energy events. We provide a workflow for applying Benford's Law to identify the onset of the motion of coarse sediment along the river bed at a time resolution of seconds. Since Benford's Law has demonstrated usefulness in acoustic amplitude analysis in this study, it could serve as a tool for identifying anomalous events in any kind of real-time data series, which could be beneficial for generating event samples for machine learning applications.

Key Points:

- Long-term, high-frequency acoustic monitoring constitutes huge-volume data sets with a low signal-to-noise ratio
- The distinct first-digit distribution between signal and noise can used to filter out 99% of background noise from acoustic recordings
- We applied the method to a three-year-long acoustic data set in Baiyang, identifying two bedload transportation events

Supporting Information:

Supporting Information may be found in the online version of this article.

Correspondence to:

C.-J. Yang,
cijianyang@ntu.edu.tw

Citation:

Yang, C.-J., Turowski, J. M., Zhou, Q., Nativ, R., Tang, H., Chang, J.-M., & Chen, W.-S. (2024). Measuring bedload motion time at second resolution using Benford's law on acoustic data. *Earth and Space Science*, *11*, e2023EA003416. https://doi.org/10.1029/2023EA003416

Received 10 NOV 2023
Accepted 9 JUL 2024

Author Contributions:

Conceptualization: Ci-Jian Yang
Data curation: Jui-Ming Chang
Formal analysis: Ci-Jian Yang
Methodology: Ci-Jian Yang, Qi Zhou
Validation: Jens M. Turowski
Writing – original draft: Ci-Jian Yang
Writing – review & editing: Ci-Jian Yang, Jens M. Turowski, Qi Zhou, Ron Nativ, Hui Tang, Wen-Sheng Chen

1. Introduction

Bedload transport driven by floods is a natural process that strongly affects the Earth's surface system. Bedload transport is a fundamental process in river corridors, with implications for channel stability (e.g., Recking et al., 2016; Turowski et al., 2009), sediment budgets (e.g., Theule et al., 2012), pollution transport (e.g., Stott et al., 2001), fluvial erosion (e.g., Turowski et al., 2008), and aquatic habitats (e.g., Snyder et al., 2009). Bedload transport increases river lateral migration or erosion and deposition, with potentially hazardous effects on downstream residents' lives and property (e.g., Bufe et al., 2019; Krapesch et al., 2011). In Switzerland, bedload transport caused cumulative financial losses of USD 5.3 billion from 1972 to 2011, about one-third of the total natural hazard damage during that period (Badoux et al., 2014). Reliable approaches for bedload monitoring are needed not only for hazard warning systems but also for quantifying fluvial processes.

Monitoring in extreme environments during storms can complement existing observations of fluvial processes, such as understanding temporal changes in bedload motion and calculating the proportion of total sediment flux. Yet, the estimations of bedload transport from long-term monitoring systems are limited. Extensive field testing has been conducted for monitoring bedload with high temporal resolution through surrogate techniques. For

instance, in the field of fluvial seismology, seismometers are deployed nearby to detect the vibration signature of bedload transport in continuous seismic records (Barrière et al., 2015; Burtin et al., 2008, 2009, 2011; Chao et al., 2015; Cook et al., 2021; Díaz et al., 2014; Dietze et al., 2019, 2022; Roth et al., 2016; Schmandt et al., 2013; Walter et al., 2017). In addition, passive acoustic methods, for example, hydrophones, and seismic instruments used, for instance, in impact plates (e.g., Rickenmann et al., 2012), are sensitive to bedload motion (e.g., Burtin et al., 2016; Geay et al., 2017, 2020). Acoustic data from hydrophones, where bedload impacts can be heard directly, provide a benchmark that is not usually available when using seismic data only (e.g., Roth et al., 2017). In addition, high-frequency acoustic monitoring allows for detecting bedload motion in realtime, which could be used for warning systems, improving over generic empirical values calibrated on previous events (Abancó et al., 2012; Badoux et al., 2014; Baum & Godt, 2010; Marra et al., 2016). However, an automatic and efficient method for constraining the onset of bedload transport events from long-term acoustic data is still lacking.

Benford's Law refers to a specific probability distribution of the first-digit of data sets. It predicts that a first digit of one occurs about 30% of the time in a given data set, three times higher than the value of 1/9 expected from a uniform distribution. Benford's Law has been used to identify fraud in accounting or political votes (Nigrini, 1999). It appears in natural data as well. For example, nearly half of a million US annual average flows and the size of global lakes and wetlands follow Benford's Law (Nigrini & Miller, 2007). Benford's Law has been used to distinguish noise from chaotic processes when the process causes higher energy events than baseline noise (Li et al., 2015). For example, the onset of earthquakes has been identified using Benford's Law on seismic amplitude data (Díaz et al., 2015; Sambridge et al., 2010). In addition, accurate and complete observational data on the traveled distance of tropical cyclones conform to Benford's Law. Thus, Benford's Law residuals become a tool for evaluating data quality and homogeneity (Joannes-Boyau et al., 2015).

In underwater acoustic recordings, the median power of bedload-generated noise in the frequency range between 10^3 Hz and 10^4 Hz is about 2.5 orders of magnitude higher than that of the low flow period at the same reach (Geay et al., 2017). Therefore, we hypothesize that the change in the first-digit distribution of acoustic amplitudes can properly identify high-energy events, and in principle, we expect that the first-digit distribution has the potential to be an indicator that can be used to separate sound categories, that is, air, waterflow, and motion of pebbles. An incomplete magnitude data range might not always result in the highest frequency of the first digit being 1 for high-energy events; for example, the 95th percentile of power spectral density ranges from 10^4 to 5×10^4 mPa^2/Hz (Geay et al., 2017). This half-order of magnitude data range results in a new first-digit distribution different from Benford's Law.

Here, we develop a simple statistical tool based on Benford's law that can automatically and efficiently identify bedload signals from long-term acoustic recordings. We apply the method to 3 years of underwater audio observations at Baiyang hydrometric station. We demonstrate the potential of Benford's Law in distinguishing sound categories.

2. Materials and Methods

2.1. Benford's Law

Benford's Law (Benford, 1938) states that the probability of the first-digit is non-uniform but rather obeys the mantissae of their logarithms, Equation 1:

$$P_D = \log_{10}\left(1 + {}^{1}\!/_{D}\right). \quad (1)$$

Here, P_D is the probability of the first-digit D occurring ($D = 1, \ldots, 9$). For example, the first-digit of -0.01, 1, or 1×10^8 are all 1. The law suggests that numbers beginning with a one occur about 30.1% of the time in some natural data sets, while those with the first-digit of two occur about 17.6% of the time, and so on, down to the first-digit of nine occurring about 4.6% of the time. Data that conforms to Zipf's law also conforms to Benford's Law (Newman, 2005). Zipf's law states that in a given data set, the frequency of an item scales inversely with its rank (Zipf, 1949). The manifestation of Benford's Law occurs precisely when the scaling exponent equals 1 (Pietronero et al., 2001; Zhou et al., 2023).

10.1029/2023EA003416

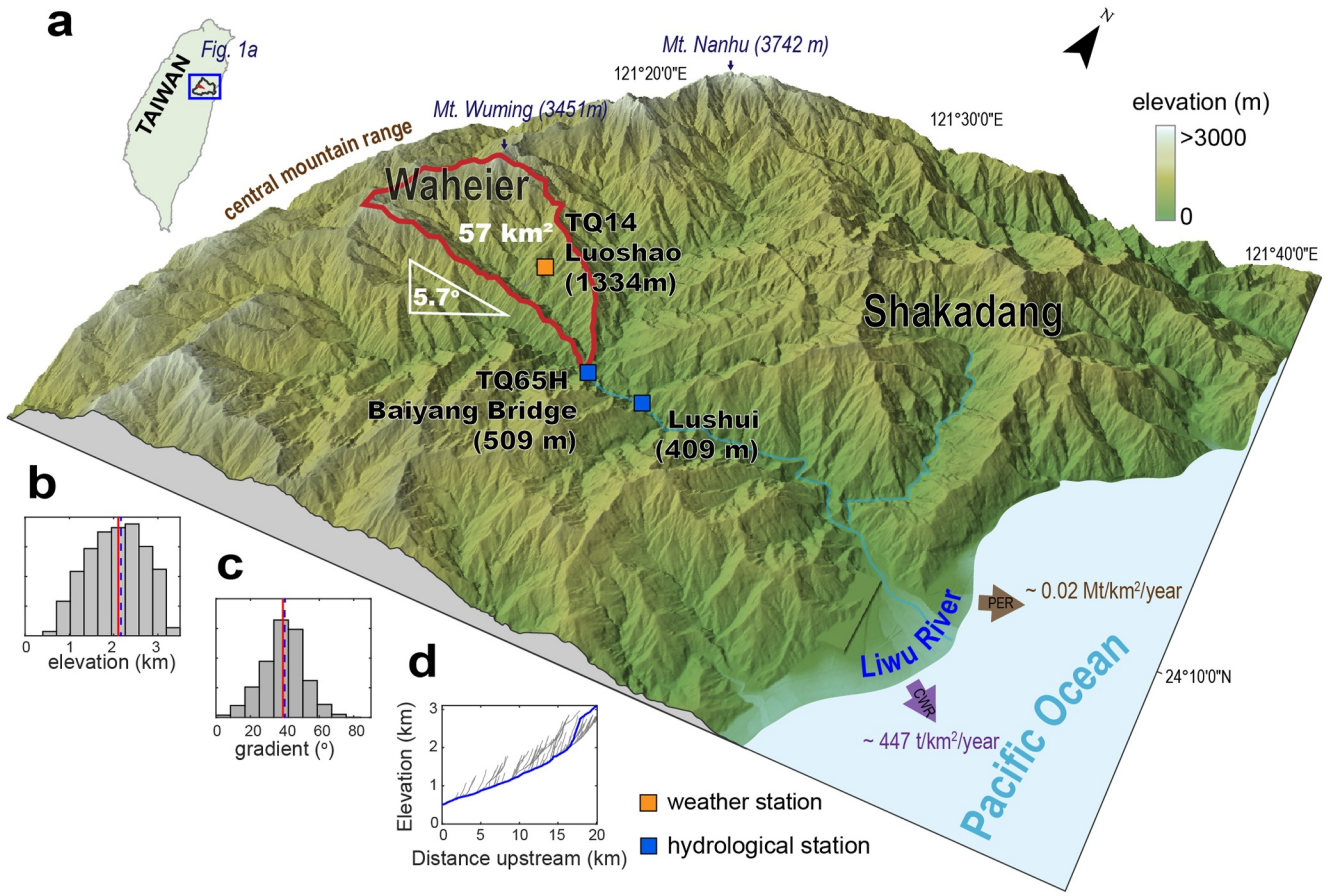

Figure 1. (a) Topographical 3D view of the Liwu catchment and the study site. In the outlet of the Waheier catchment, Baiyang hydrometric station (TQ65H) monitors river acoustic sounds and provides hydrometric data. Minute-resolution rainfall is obtained from the Luoshao (TQ14) weather station. (b) Histogram of elevation of Waheier catchment, red line denotes median value, and blue dash denotes mean value. (c) Histogram of hillslope gradient of Waheier catchment, red line denotes median value, and blue dash denotes mean value. (d) Longitudinal profile of the upstream from the Baiyang station.

We use a least squares misfit measure to quantify the discrepancy between the observed and theoretical probability of the first-digit (Joannes-Boyau et al., 2015). We subtract the misfit from one and define it as the goodness of fit (Equation 2):

$$\sigma = 1 - \sum_{(D=1)}^{9} \left(\frac{n_D}{n} - P_D \right)^2, \tag{2}$$

where P_D is the theoretical probability of amplitude of the acoustic signal with the first-digit D as given by Benford's Law, n_D is the number of amplitudes of the acoustic signal with the first-digit D, and n is the total number of data. The first-digit distribution can be independently assessed for the goodness of fit against theoretical values of Benford's Law at the second scale in this study, eliminating the need for other detecting methods or the requirement for baseline observations. In addition, we calculate the acoustic amplitude difference between the 75th and 25th percentile (interquartile range) for every second as an index of the data range.

2.2. Study Site and Monitoring

The Liwu catchment is located in eastern Taiwan (Figure 1a), experiencing high-frequency seismic activity and rapid tectonic uplift of 5.5 mm yr^{-1} (Petley et al., 1997). The mean annual rainfall is about 2.5 m, and typhoons are the dominant source of heavy rainfall, accounting for 66% of the annual discharge (Huang et al., 2012). This results in 20,000 t km^{-2} y^{-1} of physical denudation rate calculated from suspended sediment (Dadson et al., 2003) and 18 t km^{-2} y^{-1} derived from silicate weathering, which is one of highest measured so far in the world for felsic

lithologies (Calmels et al., 2011). The Liwu provides a natural laboratory with active driving forces, relatively minor human influence, and a unique opportunity to investigate bedload dynamics from a typhoon-dominated system.

Baiyang hydrometric station is located on the outlet of Waheier catchment, a tributary of Liwu River, which drains 57 km^2. Elevation in the Waheier catchment spans from 509 to 3,451 m with a mean of 2,055 m (Figure 1b). The mean hillslope gradient is 39.5° (Figure 1c), and the mean channel gradient is about 5.7%. The length of the mainstream is 20.8 km (Figure 1d). Baiyang hydrometric station was installed at Baiyang Bridge in April 2018. There, underwater acoustic noise has been continuously measured at a 32 kHz sampling rate using a broadband hydrophone with the useful range 10–10^5 Hz, Aquarian H2a-XLR (Aquarian Audio, 2013). The data logger used is a Raspberry Pi–based controller combined with a Zoom U–22 logger at resolutions up to 24-bit/96 kHz. The hydrophone is protected by a 30 cm metal tube attached to the bedrock close to the water surface at a low flow of about ∼1 m. Five-minute-resolution measurement of the water stage is measured using a Radar Level Sensor with an accuracy of 10 mm. Half-hour time-lapse imagery is recorded by three D30 Canon cameras with different viewpoints. Within the same catchment, Luoshao station (Figure 1) provides minute-resolution rainfall measurements using an automatic weather station, a Vaisala WXT-536.

2.3. Data Preparation and Audio Recording Visualization

Based on the test of statistical preprocessing, which includes detrending and deconvolution, and its impact on the distribution of the first digit of acoustic amplitude, the results indicate that there is no difference in distribution whether preprocessing is applied or not (Figure S1 in Supporting Information S1). Therefore, we did not preprocess the audio data in this study. This has the further advantage of significantly reducing the computational cost of our method. However, removing possible linear trends and zero offsets from non-zero-mean signals is still necessary. For instance, Díaz et al. (2015) implemented preprocessing steps such as detrending and demeaning on seismic data. Here, we used the acoustic recordings from the stationary hydrophone deployed from 2019 to 2022 (Figure 2a). After removing damaged and short-period files (<1 min), the total duration of acoustic recordings is 15,248 hr, which represents 58% of the overall observation period. The remaining time includes periods of damaged recordings and equipment malfunctions (Figure 3). The audio data was split into .mp3 files of 5 min in length. Each second of recording has 32,000 individual acoustic amplitude measurements, sufficient to calculate the probability distribution of the first-digit. To visualize audio recordings, we transformed the signals from the time domain to the frequency domain using a short-time Fourier transform to obtain the power spectral density by using the built-in functions in MATLAB. Due to differences in the time resolution of the audio recordings, water level, and rainfall data in this study, we harmonize the time resolution of 5 min based on the measurement resolution of the water level at Baiyang station. Then, the goodness of fit is calculated by averaging the results from the second scale to 5 min (Figures 4a and 4b), while the minute-scale rainfall amounts are accumulated into total hourly rainfall (Figures 4a and 4b). Audio recordings calculate the percentage of event signals (Figures 4c and 4d) and spectrograms (Figures 4e and 4f) over a 5-min scale. Therefore, we refer to our data as having a 5-scale because it represents the 5-min recording period itself.

2.4. Sound Classification via Residual Probability Distribution

To distinguish between different sound categories based on the probability of first-digit, our workflow contains three steps. First, we calculate the residual between the probability of first-digit for observed data and Benford's theoretical frequencies, and we categorized the residuals into two groups: event signals and background signals. We utilize the amplitude of the acoustic signal per second as the basic unit. There are 32,000 data points for each second's amplitude, allowing us to calculate the distribution of the first digits. For each second of acoustic signal, we then differentiate between event signals and background signals based on the position of the highest probability of the first digit. For example, if the highest probability occurs when the first digit is 3, the signal is defined as a background signal, while all other categories are considered event signals. Second, we identified sound categories using the *k*-means clustering and determine the number of clusters using the Elbow method (Thorndike, 1953), along with the method to assess the clustering stability. Third, we calculated the time-series ratio of respective sound categories by calculating the relative duration of the event signal for every 5-min blocks. For example, an event signal of 50% indicates that the event signal accounts for 2.5 min within a 5-min duration (Figure 3). These steps are described in detail in the supplementary.

10.1029/2023EA003416

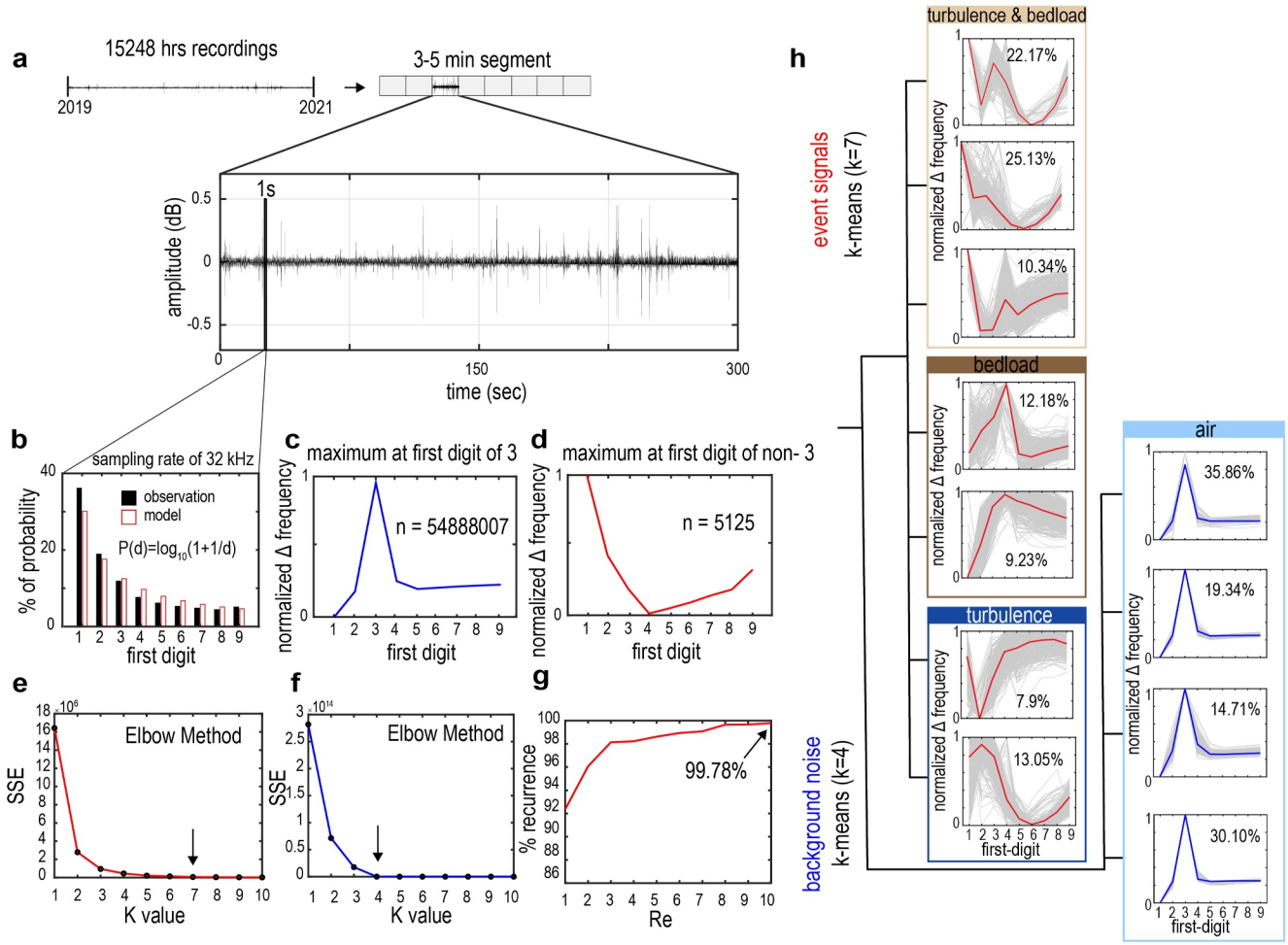

Figure 2. Workflow of the applied Benford's law to sound combinations. (a) Schematic diagram of the acoustic amplitude along the entire study period. An acoustic data file (*.mp3) is generated for every 3–5 min of acoustic recordings. (b) A comparison of the probability distribution of Benford's Law model and observation in %, P is the probability, and D is the first-digit. (c) Schematic diagram of the category of normalized probability difference with a maximum at the first-digit of three. (d) The category of normalized probability difference with a maximum is not at the first-digit of three. (e) Determining the k-value (number of clusters) of event noise according to the Elbow method. (f) Determining the k-value of background noise with the Elbow method. (g) Determining the parameter Re (number of times to repeat clustering). (h) Categories of normalized probability difference distribution, classified by the k-means method. Percentages represent proportions in the same group.

3. Results

3.1. Sound Classification Determined by k-Means Clustering

Seven classes arise from k-means clustering for event signals (n = 5,125) and four classes for background noise (n = 54,888,007). The Elbow method provides the k value to satisfy the statistical objective of minimizing within-cluster error in the k-means method, and it may lead to overfitting, surpassing the requirements for sound identification. For example, background noise can be separated into four classes, but they do not hold physical meaning. Furthermore, through direct listening and manual classification of the acoustic signal, we identified distinctive characteristics in the residual probability. Specific types of sounds exhibit the same largest residual position. For example, the largest residual value at the first-digit of three is always an air sound; the largest residual value at the first-digit of one is mainly the sound of turbulence with sediment impacts, which occurs about 57.6% of the duration of the total event signal; the largest residual value at the first-digit of four is mainly the sound of sediment impacts that are inferred to be due to bedload transport, occurring at 21.41% of the total event signal. The other two classes accounted for 20.95% in total, mostly the sound of turbulence. Notably, the largest residuals of turbulence are not in the same position. To simplify the acoustic diversity, we merged them according

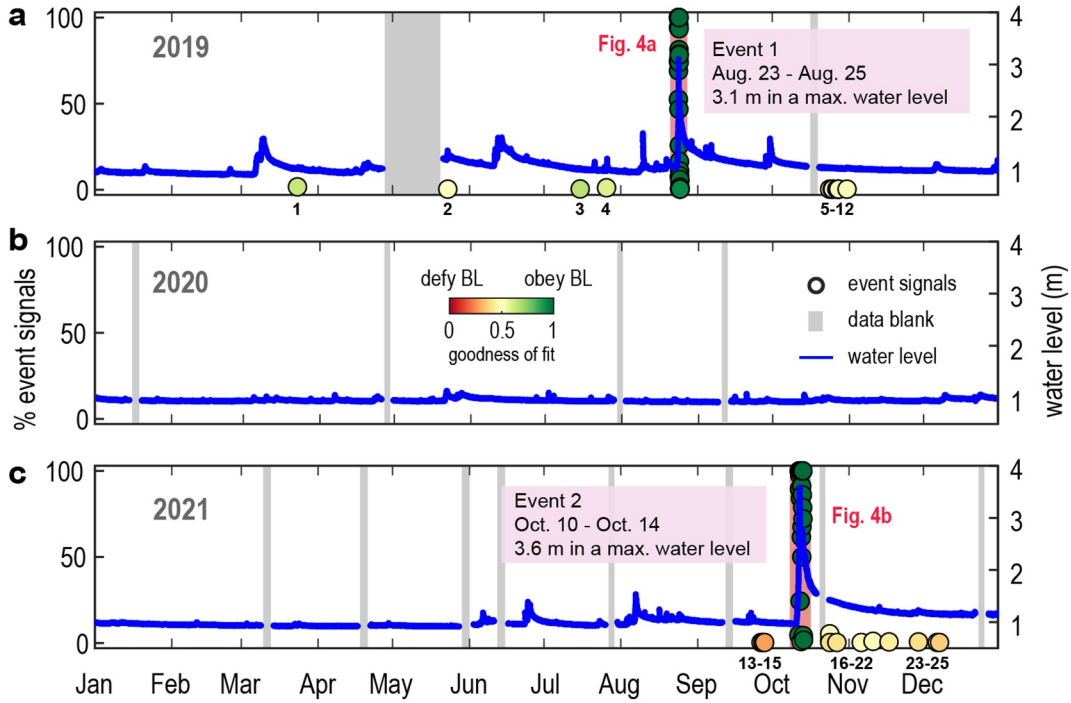

Figure 3. Three-year time series of event signal ratios, the goodness of fit, and river water levels. Panel (a–c) represents the years from 2019 to 2021. Blue lines are water hydrographs, and circles denote event signals in %, colored by the goodness of fit. Numbers beside the circles mark the misidentified 25 audio files. The gray areas represent data blanks.

to the location of the largest residual value into four classes of sounds, that is, bedload motion, turbulence with bedload motion, turbulence, and air (Figure 2h).

3.2. The Goodness of Fit Marks Bedload Transportation Events

From 2019 to 2021, two bedload transport events occurred at Baiyang station. The first event happened on 24 August 2019, with a maximum water level of 3.1 m. The goodness of fit is nearly one during this period, meaning that the first-digit distribution closely follows Bedford's law, and the ratio of event signal increases to 100% (Figure 3a). The second event happened on 10 October 2021, with a maximum water level of 3.6 m. Similarly, the goodness of fit is nearly one during this period, and the ratio of event signal increases to 100% (Figure 3c). In 2020, the water level did not exceed 1.1 m, and bedload transport was negligible (Figure 3b). Apart from these two events, 25 audio files contain event signals, accounting for 28 s, 0.54% of the total event signal. In addition, the mean amplitude difference (75th–25th) of these 25 audio files is $0.007 \pm 3 \times 10^{-5}$ dB re $(m/s)^2$/Hz, and the mean power calculated from the spectrogram is -85.21 ± 6.14 dB (Table S1 in Supporting Information S1). Given low values in duration, acoustic intensities, the goodness of fit, and the ratio of event signal, we ruled out these 25 audio recordings from bedload transport events.

3.3. Changes in Residual Probability of the First-Digit Distribution During the Two Events

Our examination demonstrates that the hydrophone captures sounds emanating from various physical mediums, including air, water flow, and bedload motion throughout the monitoring period (Figure 4). In the first event, the ratio of bedload motion occurrence increased from 7.3% at 04:50 on 24 August 2019, with a critical stage of 2.2 m, to 90.1% after 3 hr, followed by a decrease to 9.9% at 10:50 on August 24, about 6 hr later. Sounds of turbulence with sediment impact start with bedload motion but dominate the source of sound in the early and late stages of the event by over 52% of the 5-min sound contribution. Sounds reflecting sediment impact account for 82.5% of 5-min sound contribution during the peak of bedload motion. Eventually, the bedload motion ends at 21:50 on August 24, while the dominant sound contributor becomes air (background noise) (Figure 4c).

10.1029/2023EA003416

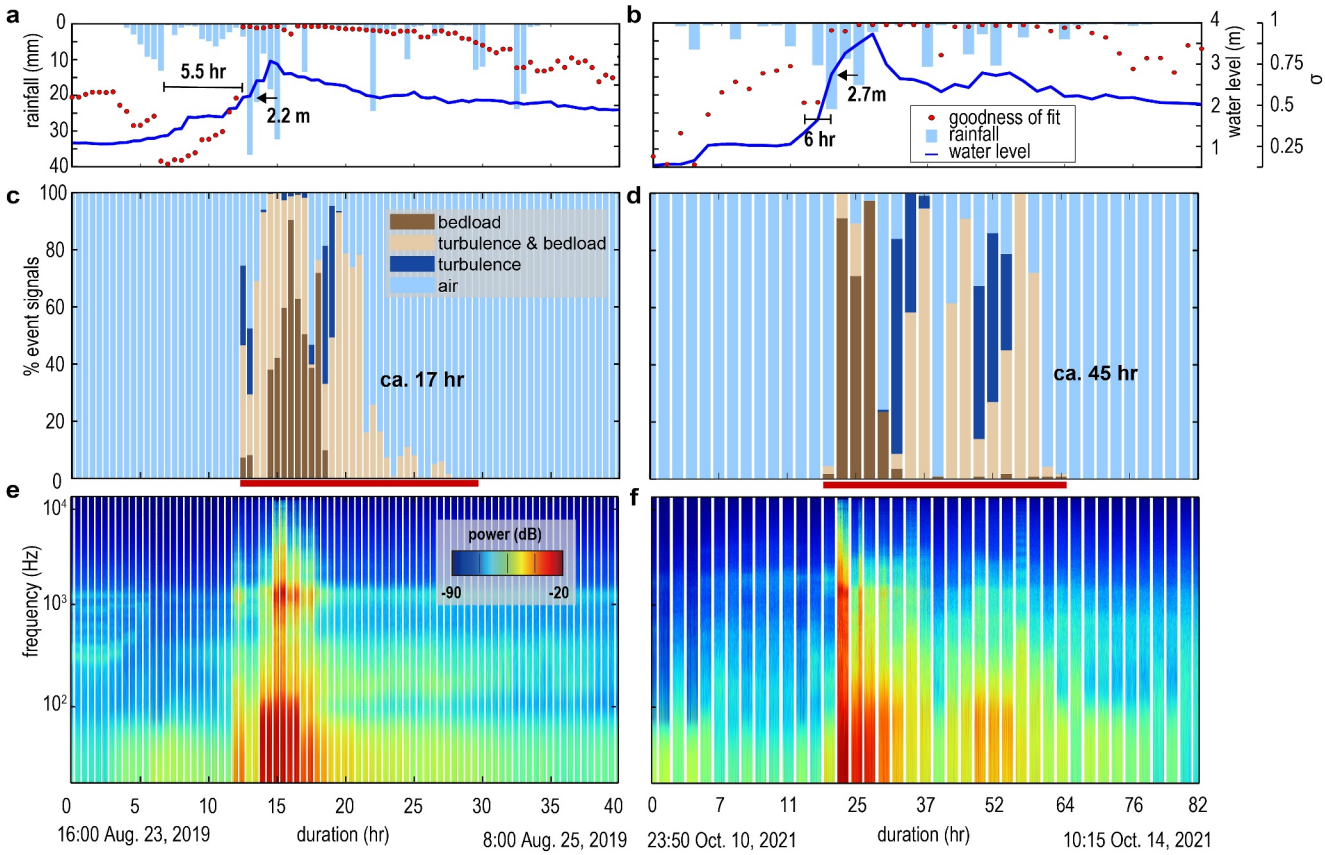

Figure 4. Sound combinations of the two bedload transportation events. (a and b) Rainfall, water level, and goodness of fit. Periods denote the duration of the decline period in goodness of fit. (c and d) Time series of sound combinations. Colors represent the source of the sound (see legend). (e and f) Semilogarithmic spectrograms of acoustic signals.

During the second event, the ratio of bedload motion in 5-min sound blocks increased from 1.8% at 18:55 on October 2021, with a critical stage of 1.9 m, to 97.4% at 03:55 on October 12 with a critical stage of 2.7 m, followed by a decrease to 3.5% at 09:55 on October 12, about 6 hr later. At the time of the local low water stage of 2.4 m, bedload motion stopped. Then, the motion restarted at a higher water level of 2.5 m with a 1% ratio of bedload motion. Similarly, the occurrence of turbulence together with bedload transport dominates the sound source in the recession limb by over 60%. By 15:55 on October 12, the sound was fully generated by air (Figure 4d). Based on the occurrence and end time of bedload signals, we calculate the duration of the two bedload transport events, yielding 17 and 45 hr, respectively, constituting roughly 30.7 hr or 0.35% of the time per year.

4. Discussion

4.1. Applications of the Acoustic and Statistical Method

We present an automatic and efficient workflow to identify the onset of bedload transport and reveal the dynamic sound combinations during sediment transport events. We have also proposed recommendations regarding data processing. The distribution of first digits in background noise may vary depending on the static voltage of the instrument, for example, loggers, seismic or acoustic stations, and the type of noise. We propose visualizing short-term audio files and applying Benford's Law to establish a connection between background noise and the distribution of first-digit, which would significantly reduce computational expenses, compared to directly calculating the entire database.

The residual probability of bedload signals appears at the location of the first-digit with four in this study, which may vary depending on the monitoring instrument, but can be verified through human listening and acoustic spectrograms. Therefore, we recommend conducting short-term validations between the residual probability and

the sound types. Although *k*-means clustering offers the advantage of fast computation, we encountered the issue of overfitting. We have merged 11 types of sounds into four types based on human listening. We recommend using supervised classification tools for distinguishing different sounds.

4.2. The Sound Combination Determined by Residual Probability Reflects Bedload Dynamics

Using the residual probability of the first-digit distribution, we classify sounds at a second timescale and accurately determine the timing and critical state for the onset of bedload motion. Sound combinations reflect dynamic flooding events where numerous processes may occur individually or concurrently (e.g., Figure 4). Moreover, the critical state of the second event is 1.24 times higher than the first event. We infer that following the bedload transport event, the bed morphology was altered, as such, gravels inlaid with each other, forming higher critical shear stress for the onset of bedload motion (cf., Turowski et al., 2011). In addition, small to intermediate past flows can increase the stability of the bed, increasing the threshold stage for the onset of motion, while high-magnitude flows decrease it (Masteller et al., 2019).

The ratio of bedload signal temporally coincides with the mean of the acoustic power calculated from the spectrogram (Figure S2 in Supporting Information S1). The spectrogram at Baiyang station on 23–25 August 2019 (Figure 4e) shows that before the onset of the bedload motion (defined by the goodness of fit; Figure 4a), the acoustic power below 100 Hz is about two orders of magnitude higher than in other frequency bands, which can be attributed to the sound of flowing water. When the bedload transport begins, the acoustic power at frequency bands of ∼1,000 Hz increases by about five orders of magnitude. This increase lasts for about six to 7 hr. The October 2021 spectrogram (Figure 4f) exhibits a similar pattern; the acoustic power increases by several orders of magnitude at high frequency. When the ratio of bedload sound decreases, the acoustic power also decreases.

4.3. Decreasing Goodness of Fit at Incipient Flooding

The goodness of fit can not only be used to identify the onset of bedload transport, but potentially also changes in hydraulics. We found that decreasing goodness of fit and increasing water level are abrupt at incipient flooding (Figures 4a and 4b). In the first event, 5.5 hr before the onset of bedload motion, the goodness of fit decreased from 0.63 to 0.45, and the water level increased conversely from 1.19 to 1.24 m. In the second event, 6 hr before bedload motion, the goodness of fit decreased from 0.79 to 0.63, and the water level increased conversely from 1.5 to 1.7 m.

We found sound sources with sound durations shorter than 1 s which we consider as pulse-type sources (Figure S3a and S3b in Supporting Information S1). The pulses may be caused by advancing flood waves, where the surging water surface entrains a large number of air bubbles, making the hydrophone susceptible to a mechanical pulse sound. The increases amplitude by less than an order of magnitude, prohibiting the full application of Benford's Law and reducing the goodness of fit. Next, we calculated the goodness of fit and magnitude of sound for the ca. 6 hr preceding the two bedload transport events, respectively (Figure S4 in Supporting Information S1). The result infer that pulse signals would decrease the goodness of fit. However, we cannot confirm that this is the only cause for the decreasing goodness of fit, as other factors causing a decrease in sound amplitude could also be contributors. Even though such pulse-type sound is defined as background noise in this study, it combines with the change in the goodness of fit, we could grasp this hydrological change. If such an abrupt decrease in the goodness of fit at the rising limb of the hydrograph is consistent throughout various study sites, it may constitute an important feature that can be utilized to improve early warning systems for Earth surface flows, including bedload transport and debris flows.

5. Conclusion

A method that can rapidly and accurately detect the onset of bedload transport in real-time is crucial for disaster warnings and calculating sediment flux. We use the probability change in the first-digit distribution–Benford's Law –from the two bedload transport events to establish a workflow flow of event detection and sound classification. With our workflow, we were able to filter out >99% of the background noise from acoustic recordings and focus on flooding event acoustic signals that can further be separated into three sound classes by statistical clustering tools. We propose a statistical "goodness of fit" between the theoretical Benford's Law and empirical data and find this parameter to match the onset of bedload motion. Hence, we propose that the operating timing of an expensive monitoring tool, for example, an automatic river water sampler, can be initiated using this simple

parameter. Benford's Law can identify the events of interest like the onset of bedload transport in the data, but it cannot classify them. As such, it can serve as a tool for labeling events for machine learning. Furthermore, goodness of fit can also be used to compare with other event detectors, or as a feature in the training of machine-learning methods. As an event detector, it can be applied simply and quickly, and, can thus be applied in near real-time to incoming monitoring data. We used the audio data at a sampling rate of 32 kHz, which is sufficient for Benford's Law calculation. Increasing the time resolution to sub-second resolutions is possible. Reducing the time resolution to the minute scale is necessary to acquire a data set with an adequate sample size and expected data range. Nonetheless, minute-scale observations are sufficient for early warning of fluvial disasters.

Data Availability Statement

All data and MATLAB code analyzed in this study are available at Yang (2023). The spectrograms for the sounds of bedload transport and background noise, including the spectrograms for bedload transport events defined in 2019 and 2021 are available at Yang (2024).

Acknowledgments
We express our gratitude to Torsten Queißer, Markus Reich, and Gunnar Pruß and other member of the Geomorphology Section at GFZ for their assistance in establishing the Taroko monitoring program. We apologize for not being able to list each individual's name. This study was supported by grants from the National Science and Technology Council of Taiwan awarded to C.-J. Yang (MOST 110-2917-I-564-009 and NSTC 112-2116-M-002-033-MY3). We express our gratitude for the constructive feedback provided by the two anonymous reviewers.

References

Abancó, C., Hürlimann, M., Fritschi, B., Graf, C., & Moya, J. (2012). Transformation of ground vibration signal for debris flow monitoring and detection in alarm systems. *Sensors*, *12*(4), 4870–4891. https://doi.org/10.3390/s120404870

Aquarian Audio. (2013). *Aquarian Audio Products H1a Hydrophone User's Guide*. Aquarian Audio Products. Retrieved from https://www.aquarianaudio.com/AqAudDocs/H1a_manual.pdf

Badoux, A., Andres, N., & Turowski, J. M. (2014). Damage costs due to bedload transport processes in Switzerland. *Natural Hazards and Earth System Sciences*, *14*(2), 279–294. https://doi.org/10.5194/nhess-14-279-2014

Barrière, J., Oth, A., Hostache, R., & Krein, A. (2015). Bed load transport monitoring using seismic observations in a low-gradient rural gravel bed stream. *Geophysical Research Letters*, *42*(7), 2294–2301. https://doi.org/10.1002/2015GL063630

Baum, R. L., & Godt, J. W. (2010). Early warning of rainfall-induced shallow landslides and debris flows in the USA. *Landslides*, *7*(3), 259–272. https://doi.org/10.1007/s10346-009-0177-0

Benford, F. (1938). The law of anomalous numbers. *Proceedings of the American Philosophical Society*, *78*(4), 551–572.

Bufe, A., Turowski, J. M., Burbank, D. W., Paola, C., Wickert, A. D., & Tofelde, S. (2019). Controls on the lateral channel-migration rate of braided channel systems in coarse non-cohesive sediment. *Earth Surface Processes and Landforms*, *44*(14), 2823–2836. https://doi.org/10.1002/esp.4710

Burtin, A., Bollinger, L., Cattin, R., Vergne, J., & Nábělek, J. L. (2009). Spatiotemporal sequence of Himalayan debris flow from analysis of high-frequency seismic noise. *Journal of Geophysical Research*, *114*(F4), F04009. https://doi.org/10.1029/2008JF001198

Burtin, A., Bollinger, L., Vergne, J., Cattin, R., & Nábělek, J. L. (2008). Spectral analysis of seismic noise induced by rivers: A new tool to monitor spatiotemporal changes in stream hydrodynamics. *Journal of Geophysical Research*, *113*(B5), B05301. https://doi.org/10.1029/2007JB005034

Burtin, A., Cattin, R., Bollinger, L., Vergne, J., Steer, P., Robert, A., et al. (2011). Towards the hydrologic and bed load monitoring from high-frequency seismic noise in a braided river: The "torrent de St Pierre", French Alps. *Journal of Hydrology*, *408*(1–2), 43–53. https://doi.org/10.1016/j.jhydrol.2011.07.014

Burtin, A., Hovius, N., & Turowski, J. (2016). Seismic monitoring of torrential and fluvial processes. *Earth Surface Dynamics*, *4*(2), 285–307. https://doi.org/10.5194/esurf-4-285-2016

Calmels, D., Galy, A., Hovius, N., Bickle, M. J., West, A. J., Chen, M.-C., & Chapman, H. (2011). Contribution of deep groundwater to the weathering budget in a rapidly eroding mountain belt, Taiwan. *Earth and Planetary Science Letters*, *303*(1–2), 48–58. https://doi.org/10.1016/j.epsl.2010.12.032

Chao, W. A., Wu, Y. M., Zhao, L., Tsai, V. C., & Chen, C. H. (2015). Seismologically determined bedload flux during the typhoon season. *Scientific Reports*, *5*(1), 8261. https://doi.org/10.1038/srep08261

Cook, K., Rekapalli, R., Dietze, M., Pilz, M., Cesca, S., Purnachandra, R., et al. (2021). Early warning of catastrophic flow events using regional seismic networks. *Science*, *374*(6563), 87–92. https://doi.org/10.1126/science.abj1227

Dadson, S. J., Hovius, N., Chen, H., Dade, W. B., Hsieh, M.-L., Willett, S. D., et al. (2003). Links between erosion, runoff variability and seismicity in the Taiwan orogen. *Nature*, *426*(6967), 648–651. https://doi.org/10.1038/nature02150

Díaz, J., Gallart, J., & Ruiz, M. (2015). On the ability of the Benford's law to detect earthquakes and discriminate seismic signals. *Seismological Research Letters*, *86*(1), 192–201. https://doi.org/10.1785/0220140131

Díaz, J., Ruíz, M., Crescentini, L., Amoruso, A., & Gallart, J. (2014). Seismic monitoring of an Alpine mountain river. *Journal of Geophysical Research: Solid Earth*, *119*(4), 3276–3289. https://doi.org/10.1002/2014JB010955

Dietze, M., Hoffmann, T., Bell, R., Schrott, L., & Hovius, N. (2022). A seismic approach to flood detection and characterization in upland catchments. *Geophysical Research Letters*, *49*(20), e2022GL100170. https://doi.org/10.1029/2022GL100170

Dietze, M., Lagarde, S., Halfi, E., Laronne, J., & Turowski, J. (2019). Joint sensing of bedload flux and water depth by seismic data inversion. *Water Resources Research*, *55*(11), 9892–9904. https://doi.org/10.1029/2019WR026072

Geay, T., Belleudy, P., Gervaise, C., Habersack, H., Aigner, J., Kreisler, A., et al. (2017). Passive acoustic monitoring of bed load discharge in a large gravel bed river. *J. Geophys. Res.Earth Surface*, *122*(2), 528–545. https://doi.org/10.1002/2016JF004112

Geay, T., Zanker, S., Misset, C., & Recking, A. (2020). Passive acoustic measurement of bedload transport: Toward a global calibration curve? *Journal of Geophysical Research: Earth Surface*, *125*(8), e2019JF005242. https://doi.org/10.1029/2019JF005242

Huang, J.-C., Yu, C.-K., Lee, J.-Y., Cheng, L.-W., Lee, T.-Y., & Kao, S.-J. (2012). Linking typhoon tracks and spatial rainfall patterns for improving flood lead time predictions over a mesoscale mountainous watershed. *Water Resources Research*, *48*(9), W09540. https://doi.org/10.1029/2011WR011508

Joannes-Boyau, R., Bodin, T., Scheffers, A., Sambridge, M., & May, S. M. (2015). Using Benford's law to investigate Natural Hazard dataset homogeneity. *Scientific Reports*, *5*(1), 12046. https://doi.org/10.1038/srep12046

Krapesch, G., Hauer, C., & Habersack, H. (2011). Scale orientated analysis of river width changes due to extreme flood hazards. *Natural Hazards and Earth System Sciences*, *11*(8), 2137–2147. https://doi.org/10.5194/nhess-11-2137-2011

Li, Q., Fu, Z., & Yuan, N. (2015). Beyond Benford's law: Distinguishing noise from chaos. *PLoS One*, *10*(6), e0129161. https://doi.org/10.1371/journal.pone.0129161

Marra, F., Nikolopoulos, E. I., Creutin, J. D., & Borga, M. (2016). Space–time organization of debris flows-triggering rainfall and its effect on the identification of the rainfall threshold relationship. *Journal of Hydrology*, *541*, 246–255. https://doi.org/10.1016/j.jhydrol.2015.10.010

Masteller, C. C., Finnegan, N. J., Turowski, J. M., Yager, E. M., & Rickenmann, D. (2019). History-dependent threshold for motion revealed by continuous bedload transport measurements in a steep mountain stream. *Geophysical Research Letters*, *46*(5), 2583–2591. https://doi.org/10.1029/2018GL081325

Newman, M. E. J. (2005). Power laws, Pareto distributions and Zipf's law. *Contemporary Physics*, *46*(5), 323–351. https://doi.org/10.1080/00107510500052444

Nigrini, M. (1999). I've got your number: How a mathematical phenomenon can help CPAS uncover fraud and other irregularities. *Journal of Accountancy*, 1–7.

Nigrini, M. J., & Miller, S. J. (2007). Benford's law applied to hydrology data—Results and relevance to other geophysical data. *Mathematical Geology*, *39*(5), 469–490. https://doi.org/10.1007/s11004-007-9109-5

Petley, D. N., Liu, C.-N., & Liou, Y.-S. (1997). Geohazards in a Neotectonic Terrain, Taroko Gorge, eastern Taiwan. *Memoir of the Geological Society of China*, *40*, 135–154.

Pietronero, L., Tosatti, E., Tosatti, V., & Vespignani, A. (2001). Explaining the uneven distribution of numbers in nature: The laws of Benford and Zipf. *Physica A: Statistical Mechanics and its Applications*, *293*(1–2), 297–304. https://doi.org/10.1016/S0378-4371(00)00633-6

Recking, A., Piton, G., Vazquez-Tarrio, D., & Parker, G. (2016). Quantifying the morphological print of bedload transport. *Earth Surface Processes and Landforms*, *41*(6), 809–822. https://doi.org/10.1002/esp.3869

Rickenmann, D., Turowski, J. M., Fritschi, B., Klaiber, A., & Ludwig, A. (2012). Bedload transport measurements at the Erlenbach stream with geophones and automated basket samplers. *Earth Surface Processes and Landforms*, *37*(9), 1000–1011. https://doi.org/10.1002/esp.3225

Roth, D. L., Brodsky, E. E., Finnegan, N. J., Rickenmann, D., Turowski, J. M., & Badoux, A. (2016). Bed load sediment transport inferred from seismic signals near a river. *J. Geophys. Res.Earth Surface*, *121*(4), 725–747. https://doi.org/10.1002/2015JF003782

Roth, D. L., Finnegan, N. J., Brodsky, E. E., Rickenmann, D., Turowski, J., Badoux, A., & Gimbert, F. (2017). Bed load transport and boundary roughness changes as competing causes of hysteresis in the relationship between river discharge and seismic amplitude recorded near a steep mountain stream. *Journal of Geophysical Research*, *122*(5), 1182–1200. https://doi.org/10.1002/2016JF004062

Sambridge, M., Tkalčić, H., & Jackson, A. (2010). Benford's law in the natural sciences. *Geophysical Research Letters*, *37*(22), L22301. https://doi.org/10.1029/2010GL044830

Schmandt, B., Aster, R. C., Scherler, D., Tsai, V. C., & Karlstrom, K. (2013). Multiple fluvial processes detected by riverside seismic and infrasound monitoring of a controlled flood in the Grand Canyon. *Geophysical Research Letters*, *40*(18), 4858–4863. https://doi.org/10.1002/grl.50953

Snyder, N. P., Castele, M. R., & Wright, J. R. (2009). Bedload entrainment in low-gradient paraglacial coastal rivers of Maine, U.S.A. Implications for habitat restoration. *Geomorphology*, *103*(3), 430–446. https://doi.org/10.1016/j.geomorph.2008.07.013

Stott, T., Leeks, G., Marks, S., & Sawyer, A. (2001). Environmentally sensitive plot-scale timber harvesting: Impacts on suspended sediment, bedload and bank erosion dynamics. *Journal of Environmental Management*, *63*(1), 3–25. https://doi.org/10.1006/jema.2001.0459

Theule, J. I., Liébault, F., Loye, A., Laigle, D., & Jaboyedoff, M. (2012). Sediment budget monitoring of debris-flow and bedload transport in the Manival Torrent, SE France. *Natural Hazards and Earth System Sciences*, *12*(3), 731–749. https://doi.org/10.5194/nhess-12-731-2012

Thorndike, R. L. (1953). Who belongs in the family? *Psychometrika*, *18*(4), 267–276. https://doi.org/10.1007/BF02289263

Turowski, J. M., Badoux, A., & Rickenmann, D. (2011). Start and end of bedload transport in gravel-bed streams. *Geophysical Research Letters*, *38*(4), L04401. https://doi.org/10.1029/2010GL046558

Turowski, J. M., Hovius, N., Meng-Long, H., Lague, D., & Men-Chiang, C. (2008). distribution of erosion across bedrock channels. *Earth Surface Processes and Landforms*, *33*(3), 353–363. https://doi.org/10.1002/esp.1559

Turowski, J. M., Yager, E. M., Badoux, A., Rickenmann, D., & Molnar, P. (2009). The impact of exceptional events on erosion, bedload transport and channel stability in a step-pool channel. *Earth Surface Processes and Landforms*, *34*(12), 1661–1673. https://doi.org/10.1002/esp.1855

Walter, F., Burtin, A., McArdell, B., Hovius, N., Weder, B., & Turowski, J. (2017). Testing seismic amplitude source location for fast debris-flow detection at Illgraben, Switzerland. *Natural Hazards and Earth System Sciences*, *17*(6), 939–955. https://doi.org/10.5194/nhess-17-939-2017

Yang, C. (2023). Yang et al_hy_Data [Dataset]. *Figshare*. https://doi.org/10.6084/m9.figshare.24493273.v1

Yang, C. (2024). spectrograms for sound of bedload transport and background noise [Dataset]. *Figshare*. https://doi.org/10.6084/m9.figshare.25459096.v1

Zhou, Q., Tang, H., Turowski, J. M., Braun, J., Dietze, M., Walter, F., et al. (2023). Benford's law as mass movement detector in seismic signals. *ESS Open Archive*. https://doi.org/10.22541/essoar.168987133.36073109/v1

Zipf, G. K. (1949). *Human behavior and the principle of least effort* (p. 573). Addison-Wesley.